

Onset and growth of conduction in polyimide Kapton induced by swift heavy-ion irradiation

J-P. Salvetat,* J-M. Costantini, and F. Brisard

Service de Physique et Techniques Nucléaires, Commissariat à l'Energie Atomique, BP 12, F-91680, Bruyères-le-Châtel, France

L. Zuppiroli

Laboratoire de Physique des Solides Semi-cristallins, IGA/DP, Ecole Polytechnique Fédérale de Lausanne, CH-1015, Lausanne, Switzerland

(Received 28 May 1996; revised manuscript received 15 November 1996)

In order to follow the insulator to conductor transition in a polymer when it is subject to a progressive degradation process, we have irradiated about 50 samples of poly(imide) Kapton with heavy ions and measured their conductivities as functions of temperature, electric field, and frequency. Electron spin resonance measurements gave the spin susceptibility, linewidth, g factor, and relaxation times along each step of transforming the conductivity of the material. We defined a single damage parameter that characterizes a unique damage scale for the four different ions and the different irradiation energies that we used. From the point of view of the electronic properties, the degradation process consists mainly of the nucleation and growth of carbon disordered clusters which are rich in π -conjugated bonds. During the transformation, the conductivity reflects the competition between two contributions, one of which is related to an initial disordered irradiation-doped polymeric substrate and the second to a hopping network progressively built from the merging of the clusters. The initial substrate contribution, visible in the first stage of irradiation, corresponds to a simple temperature-activated behavior and to a clear Poole-Frenkel dependence with the electric field, while the latter shows all the features of nonadiabatic hopping in a granular system. Adiabatic hopping within the clusters invades progressively all the sample in the final stage. [S0163-1829(97)07309-8]

I. INTRODUCTION

Since the late 1950s and early 1960s, solid state chemists and physicists have been interested in the thermal process of transforming organic materials into carbon. In the comprehensive review article "The chemistry of the Pyrolytic conversion of organic compounds to carbon" by Fitzer, Mueller, and Schaefer (1971), the qualitative nature of the transformation is already reasonably understood.¹ Thereafter, electron spin resonance (ESR) and dc-conductivity measurements were also performed in these disordered materials in order to follow the insulator-conductor transition.²

Many years later, ion irradiation was also used to create charge carriers in organic insulating materials through a degradation process.³ The potential applications of this process for the microelectronic industry or in the design of microwave-absorbing layers have stimulated a large amount of work in this area (see, for example, the review of Venkatesan *et al.*⁴).

Interest in the physics of electron transport in these materials increased markedly when, in 1980, Brom *et al.* made a detailed comparison between the properties of pyrolyzed Kapton and those of doped polyacetylene.⁵ At that time, most of the interpretations regarding the electronic properties of these disordered materials did not only refer to small graphite clusters as in previous interpretations, but also to disordered conducting polymers as well. These interpretations are discussed extensively in the literature. Here we summarize a few ideas that have gained wide acceptance in the field.⁴

The first stage of the polymer degradation that creates deep states in the gap of the initial insulating polymer is the

production of dangling bonds and free radicals. At this stage, resistivity is still very high, but ESR, optics, and many other more chemical techniques allow an accurate probing of this process. The second stage occurs when most of the gases such as hydrogen have left the polymer: Dangling bonds can thus recombine into some kind of disordered network of π -conjugated bonds. At this stage, room temperature (RT) conductivity is of the order of 1 S/cm and the temperature dependence of the dc conductivity varies as $\exp[-(T_0/T)^{1/2}]$, which is usually attributed to the inhomogeneous character of this network leading to a granular material. A third stage is usually ascribed to the recrystallization of the material into more "metallic" graphitic clusters.

Although some of the results could suggest a kind of an insulator-conductor transition in which the polymer band gap progressively closes and a high density of states at the Fermi level is created, many questions still remain unanswered.

Classical interpretations are always based on a single-electron picture. It is well known in disordered conducting polymers, which are also based on networks of σ and π carbon bonds, that polaronic species appear due to a strong effective electron-phonon coupling.⁶ Are these excitations important in this case? Recent models of conducting polymers also include an on-site Coulomb interaction of the order of $U \sim 5-10$ eV on a single carbon site and $U \sim 1-2$ eV on a conjugated phenyl ring.⁷ Is this interaction crucial in the picture of the insulator to conductor transition in these materials?

Most authors studying the electron transport in these systems use classical hopping models such as variable-range hopping⁸ or granular models⁹ without considering the precise nature of the hopping process: Is it adiabatic or not? Is it a

TABLE I. Film thicknesses (h), mean electronic (Se), and nuclear (Sn) stopping powers, mean projected ranges (R_p), and effective track radii (R_t) in poly(imide) Kapton-H (density $\rho=1.43$ g cm $^{-3}$).

Ion	h (μm)	ρSe (MeV μm^{-1})	ρSn (meV μm^{-1})	R_p (μm)	R_t (nm)
60 MeV ^{63}Cu	7.5	5.4 \pm 0.6	3×10^{-2}	14.5	2.3
50 MeV ^{32}S	7.5	3.3 \pm 0.1	7×10^{-3}	17.4	1.6
30 MeV ^{19}F	12.5	1.56 \pm 0.03	2×10^{-3}	20.2	0.8
30 MeV ^{12}C	12.5	0.6 \pm 0.01	4×10^{-4}	39.5	0.35

multiphonon or a single-phonon process like in the model of Miller and Abrahams?¹⁰ In this work, we attempt to address these issues and to provide partial answers to these questions.

For this purpose, we gathered an extensive and consistent set of data from about 50 irradiated samples. ESR and dc and ac conductivity measurements have been performed on each of them. While the damage produced in the track of each incident ion is obviously not known in detail, our knowledge of the radiation damage process is sufficient to provide a good damage scale for all our samples. The effect of oxygen both on the transport properties and the spin susceptibility was also studied carefully. Even though the effect of oxygen is well known on carbon-based materials (a long time ago in organic chars¹¹ and more recently in polyacetylene¹² and fullerenes¹³), to our knowledge these effects have never been clearly addressed in irradiation-damaged carbon-based materials.

Finally, this set of recent data was analyzed according to new ideas which recently have been shown to be relevant for the study of disordered conducting polymers.¹⁴ The insulator-conductor transition in PMDA-ODA polyimide (Kapton-H) induced by ion irradiation was first investigated by Hioki and co-workers^{15,16} with high-energy N_2^+ ions under implantation conditions. The present work extends significantly their results in order to provide a deeper understanding of charge and spin dynamics at each stage of the insulator-conductor transition.

II. IRRADIATION DAMAGE SCALE AND THE EFFECTS OF OXYGEN

The heavy ions used in the present work to damage the samples, the characteristics of which are reported in Table I, have been accelerated in the MeV amu $^{-1}$ range in order to traverse the whole sample. Energy was then lost essentially in the sample by an electronic slowing down process. The stopping powers $\rho Se = -(dE/dx)_{\text{el}}$ (ρ being the polymer mass density), representing the average energy loss rate of the ion along its trajectory by electronic excitations and ionizations, ranged from 600 eV nm $^{-1}$ for 30 MeV ^{12}C to 5400 eV nm $^{-1}$ for 60 MeV ^{63}Cu . With such high-energy deposition, local chemistry occurs along the ion trajectory and the ions are well known to leave tracks of transformed material within the pristine polymer.¹⁷ We found that the lateral limit of the track corresponds approximately to a local threshold of deposited energy of about 14 eV nm $^{-1}$, below which no significant damage results in the polymer.¹⁸ Thus a model of saturated track leads to the determination of track radii (of about 1 nm), which increase rather linearly with the stopping power ($R_t \propto Se$). Then the total damage left in an individual

track, per unit length, is just proportional to R_t^2 , i.e., proportional to Se^2 . The model is compatible with calculations of the radial energy distribution.¹⁸ Thus an appropriate parameter representing the primary damage in the sample is not just the fluence Φt (number of ions per unit surface), but the product $\Phi t Se^2$, which permits a rescaling of the different ion irradiations. All experimental data corresponding to a given measurement merge on a single curve independently of the incident ion, when the parameter $\Phi t Se^2$ is used instead of the simple absorbed dose $\Phi t Se$.^{18,19} In the rest of this work, this damage parameter $\Phi t Se^2$ will be used most of the time as the abscissa of our curves, which permits an illustration that is independent of the precise characteristics of the incident ions and the details of the interactions.

Oxygen is well known to act as a trap for carriers in conducting polymers¹² as well as fullerenes.¹³ Thus the results obtained with samples exposed to oxygen are very different from those corresponding to samples irradiated and measured in vacuum or in inert gases. In fact, the insulator to conductor transition is delayed in the presence of oxygen, but it does not modify the main trends.¹⁹ Fortunately, in most cases, the effect of oxygen is reversible and this gas can be eliminated by heating up to 120–150 °C under vacuum for several hours. All our measurements shown below were done in oxygen-free atmosphere.

III. EXPERIMENTAL DETAILS

A. Irradiations

Thin poly(imide) Kapton-H films were irradiated with swift heavy ions (^{12}C , ^{19}F , ^{32}S , ^{63}Cu) in the MeV amu $^{-1}$ range at room temperature under high vacuum (5×10^{-7} mbar). The ion beams were delivered by the 7-MV Van de Graaff tandem accelerator at CEA Bruyères-le-Châtel. An electrostatic scan ensured a homogeneous irradiation of the targets. Beam currents were limited below 30 nA for S and Cu ions and 100 nA for C and F ions to avoid any macroscopic heating of the target. Fluences were measured by counting the backscattered ions from a 100-nm gold layer deposited on aluminum masks or directly on the samples. Calibration was achieved by measuring the beam current with a Faraday cup. This ensured a 10% relative accuracy. Film thicknesses (7.5 and 12.5 μm) were such that the ions were transmitted through the targets. Energy was then lost essentially by an electronic slowing down process along the ion trajectory. The stopping powers calculated by the TRIM-90 code²⁰ ranged from 600 eV nm $^{-1}$ for 30 MeV ^{12}C to 5400 eV nm $^{-1}$ for 60 MeV ^{63}Cu and varied only by 10–20% along the ion path. The main characteristics of the ion beams are displayed in Table I.

B. Electrical measurements

RT ac and dc measurements were taken inside and/or outside the irradiation chamber under vacuum or under various air, oxygen, nitrogen, and helium pressures. Transverse (capacitor) and longitudinal (gap configuration) two-point dc resistances were measured. Ohmic contacts between copper wires and vacuum-deposited gold electrodes were done with silver paste. The electric field dependence was measured in the transverse geometry, which permits dc fields as high as 10^6 V cm^{-1} .

ac measurements were performed with an HP-4192A impedance meter between 10 Hz and 1 MHz. The temperature dependence of the resistance and dielectric properties were measured outside the irradiation chamber under vacuum in the 150–450 K range or in a liquid helium or nitrogen cryostat down to 1.5 K.

C. ESR measurements

After irradiation, an inert gas (N_2 or He) was introduced into the chamber to restore the atmospheric pressure and manipulate the samples. The irradiated specimens were quickly inserted into a quartz tube, which was then evacuated to prevent prolonged contact with air. This procedure required less than 2 min. Tests under various atmospheres could then be performed.

The RT ESR measurements were carried out mostly with a Varian *E*-line X-band spectrometer, operating with a double cavity. A lock-in detection was employed with four available modulation frequencies (270 Hz, 1 kHz, 10 kHz, 100 kHz). Comparison with calibrated samples guarantees very good accuracy in susceptibility and *g*-factor measurements. Spin-lattice relaxation times were deduced mainly from continuous saturation experiments on nearly homogeneous lines. RT *Q*-band experiments were performed on a Bruker apparatus to test the frequency sensitivity of the inhomogeneous linewidth. The temperature dependence of the various features (especially susceptibility and linewidth) was recorded with a Bruker X-band spectrometer equipped with a liquid helium cryostat.

IV. MAIN EXPERIMENTAL RESULTS

In Fig. 1 we report the RT conductivity $\sigma_{300 \text{ K}}$ [Fig. 1(a)], the density of paramagnetic centers, D_v , and the ESR linewidth [Fig. 1(b)] for several samples as a function of the damage parameter $\Phi t S e^2$ defined here above. The data depict a 16 orders of magnitude-change of the room temperature conductivity and a corresponding two orders of magnitude in the paramagnetic center density as a function of the damage parameter. The consideration of these three curves together permits a clear identification of four regimes numbered I, II, III, and IV in the figures.

(i) In stage I, where no significant conductivity has yet appeared, isolated paramagnetic centers are produced proportional to the damage parameter $\Phi t S e^2$.

(ii) In stage II, the conductivity increases abruptly; the typical volume fraction of irradiated samples at this stage is 50%; one can speak about some kind of percolation through the sample (we do not use this word here to describe a critical phenomenon²¹). The narrowing of the ESR line during

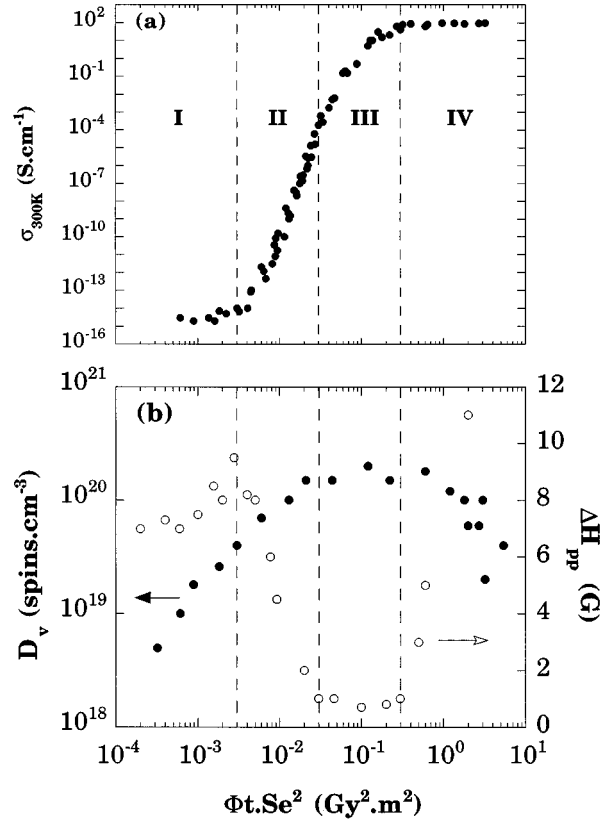


FIG. 1. (a) The RT conductivity ($\sigma_{300 \text{ K}}$) and (b) the paramagnetic center density (D_v) and the peak-to-peak ESR linewidth ($\Delta H_{p.p.}$) are plotted vs the irradiation parameter, i.e., the fluence (Φt) times the square of electronic energy loss ($S e^2$) for different ions and energies (see Table I). The insulator-conductor transition in poly(imide) Kapton proceeds along four stages, which are marked by vertical dashed lines. In stage I the damage is limited to the single-ion tracks. The onset and growth of the conduction in stages II and III are related to the damaged volume fraction by a percolation mechanism. In these stages $\Delta H_{p.p.}$ decreases. Stage IV corresponds to the saturation of the conductivity at a level close to that of polycrystalline graphite, the spin pairing leads to a clear decrease of D_v , and $\Delta H_{p.p.}$ increases due to adiabatic hopping of polaronic carriers.

this stage II ($\Delta H_{p.p.}$ decreases from 9 to 1 G) reveals some exchange (or motion) of spins.

(iii) In stage III, the slope of the conductivity versus the irradiation parameter decreases slightly; we will see further on that the conduction mechanism is different than in stage II. A saturation of the paramagnetic center density is measured, and the ESR linewidth remains constant of the order of 1 G.

(iv) In stage IV, the saturation of the conductivity to a value of about 100 S cm^{-1} is accompanied by a singlet pairing of a significant fraction of the spins.

We emphasize that Fig. 1 contains experimental points concerning irradiations with four different ions. They all merge on single curves provided that the damage parameter $\Phi t S e^2$ is used.

The temperature and field dependences of the dc conductivity also contain important information about the transport

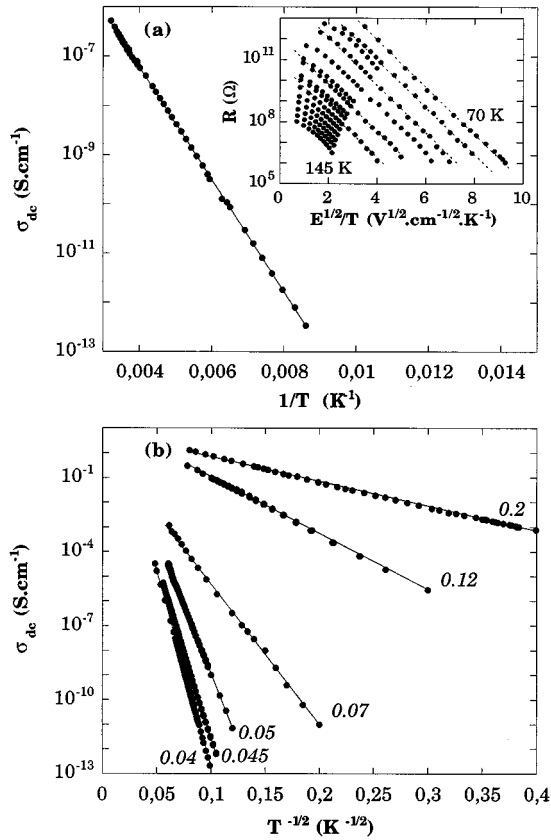


FIG. 2. (a) Typical behavior of the electrical conductivity in stage II. The logarithm of the dc conductivity is plotted vs T^{-1} , showing a simple activated behavior. The inset shows the dependence of the sample resistance vs $E^{1/2}/T$, which is characteristic of a Poole-Frenkel mechanism. The sample has been irradiated with 50 MeV S ions ($\Phi t S e^2 = 1.35 \times 10^{-2} \text{ Gy}^2 \text{ m}^2$). (b) The logarithm of the dc conductivity is plotted vs $T^{-1/2}$ for a series of samples in stage III of the transition. These linear plots are typical of granular metals. Here the “metallic” grains are conjugated π clusters where the conduction proceeds by adiabatic hopping. The slope T_0 decreases inversely with the fluence from 1.4×10^5 to 50 K. The values of the irradiation parameter are quoted in the figure.

process. Figure 2(a) represents a simple activated behavior of the conductivity

$$\sigma = \sigma_0 \exp\left(\frac{-\alpha + \beta\sqrt{E}}{k_B T}\right),$$

and the field dependence shown in the inset gives a typical Poole-Frenkel behavior^{22,23} during the stage II of irradiation (the field E was varied from 100 to 10^6 V cm^{-1} , the temperature between 70 and 145 K). Increasing further the irradiation dose (stage III), the conduction mechanism changes as illustrated in Fig. 2(b): The well-known $\sigma = \sigma_0 \exp[-(T_0/T)^{1/2}]$ hopping behavior^{5,9} is observed.

Figure 3 represents typical dielectric constant and ac conductivity curves recorded between 100 Hz and 1 MHz, at temperatures between 105 and 310 K, for a sample of stage II exhibiting already a significant dc conductivity

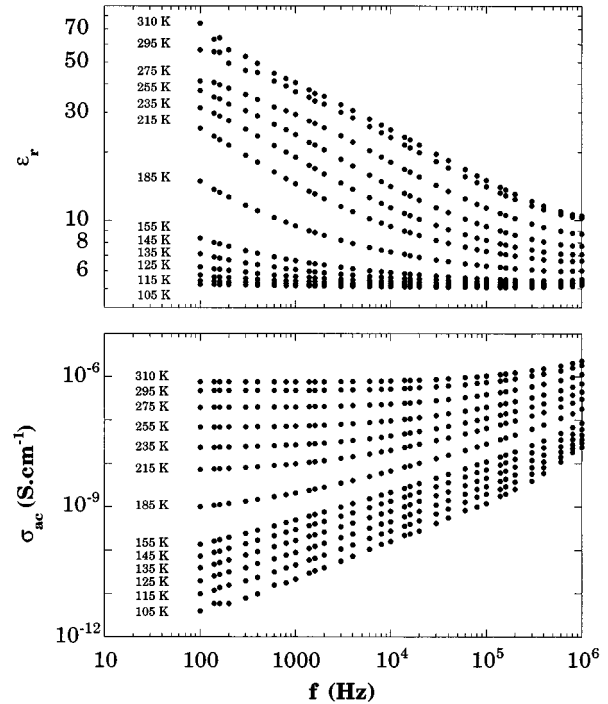


FIG. 3. The dielectric constant and ac conductivity are plotted vs frequency at various temperatures (stage II of the transition). The sample used here has been irradiated with 50 MeV S ions, $\Phi t S e^2 = 1.35 \times 10^{-2} \text{ Gy}^2 \text{ m}^2$. This behavior is typical of disordered solids.

($3 \times 10^{-3} < \Phi t S e^2 < 3 \times 10^{-2}$). The discussion will reveal that this behavior is characteristic for disordered or inhomogeneous semiconductors.

Figure 4 represents the spin susceptibility of three samples irradiated at the respective irradiation parameter $\Phi t S e^2 = 0.2, 0.5,$ and $3 \text{ Gy}^2 \text{ m}^2$. In the last stage the spin susceptibility departs from a Curie law in the high-temperature range ($T > 200 \text{ K}$). The upturn at high irradiation doses and high temperatures will be explained in the last part of the discussion.

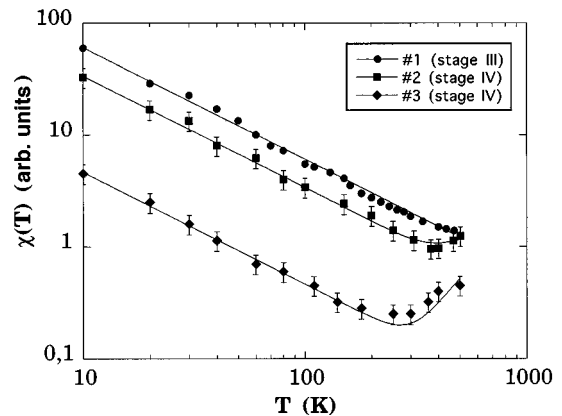


FIG. 4. The spin susceptibility χ of three samples in stages III and IV have been measured as a function of the temperature T . The irradiation parameter is 0.2, 0.5, and $3 \text{ Gy}^2 \text{ m}^2$ for samples 1, 2, and 3, respectively. The solid lines correspond to a fit using the model discussed in the text.

For the sake of clarity, part of the results will be presented together with the discussion.

V. BRIEF REVIEW OF THE MAIN MODELS OF INTEREST

A. Hopping models

When the disordered network of π -conjugated bonds extends over the sample, the conductivity must be understood in terms of hopping. It is a phonon-assisted tunneling between localized states. The solution of the whole conduction problem involves the understanding of two basic processes: local jumping between adjacent sites and ‘‘percolation’’ through the whole sample. More precisely, once the local jumping problem has been solved for each pair of sites, the carrier transport is reduced to a random walk in a random medium.

Instead of immediately invoking traditional interpretations like variable-range hopping²⁴ as well as Coulomb gap models,²⁵ it is important to define somewhat better the ‘‘hopping ground.’’ As suggested by other authors, we believe that in the present materials this ground is not really homogeneous. In fact, it is composed of clusters of sites connected by typical π transfer integrals of about 2 eV. These clusters or granules, the size of which will grow all along the irradiation, are not necessarily only ordered graphite particles and may also include localized electronic states; nevertheless, the π -conjugated bonds ensure a good transfer t_c between these states inside the disordered clusters. At the border of these clusters, which we can define as the ensemble of sites which are not connected to the outside by such π bonds, the interruption of the conjugation has drastic consequences on the hopping. There, the transfer integrals have typical values t_b of a few hundredths of eV. In the former case (t_c) hopping is adiabatic, while in the latter case (t_b) it is nonadiabatic. What is this important distinction? Our discussion will be based on the works of Holstein²⁶ and Emin.²⁷

A hop between two localized electronic states occurs when (as a result of the electron-lattice interaction) the atomic vibratory motion changes the relative energy of these localized states. For an adiabatic hop, the electron transfer energy between the sites involved in a hop is large enough (typically is greater than phonon energy) so that the electronic carrier follows the changing atomic configuration. Since the electronic carrier in an adiabatic-hop always follows the atomic motion, the jump rate in this regime is not limited by the magnitude of the electronic transfer energy. Indeed, the phonon-assisted jump rate in the adiabatic regime only depends on parameters which define the atomic motion and the electron-lattice coupling. In the complementary situation, the nonadiabatic regime, the electronic transfer energy between the two sites is so small (less than phonon energy) that the electronic carrier can only occasionally respond to favorable changes of atomic configuration by moving between sites. In these instances, the jump rate is limited by the magnitude of the electronic transfer energy. In particular, in these situations the transition rate is proportional to the square of the electronic transfer energy associated with the pair of sites as in the famous Miller-Abrahams jump rate which is widely used in hopping problems:²⁸ $\Gamma_{ij} = \gamma t_{ij}^2 \exp[-(\Delta_{ij}/k_B T)]$, where t_{ij} is the electronic trans-

fer energy associated with the pair of centers and Δ_{ij} is the energy related to the relative position of the localized levels with respect to the Fermi energy. Through $t_{ij} = t_0 \exp(-R_{ij}/L)$, the hopping rate depends on the relative distance R_{ij} between the hopping centers (L is a localization length). Thus the nonadiabatic jump rate falls with increasing intersite separation, while in the adiabatic jump the distance between sites does not appear explicitly in the rates.

It is clear, by using, for instance, the percolation argument of Ambegaokar, Halperin, and Langer,²⁹ that these difficult nonadiabatic jumps do dominate the resistance of the sample. If we believe that Coulomb interactions play a non-negligible role in these disordered carbonaceous materials of interest here, this intercluster hopping can be calculated according to the granular model of Sheng, Abeles, and Arie,³⁰ which has been extended recently to the case of disordered conducting polymers by one of us (L.Z.).¹⁴ This will explain the temperature dependence of the conductivity $\sigma = \sigma_0 \exp[-(T_0/T)^{1/2}]$ observed in Fig. 2(b).

B. Poole-Frenkel regime

In the beginning of stage II (when the volume fraction $P = \Phi t \pi R_i^2$ of the damaged material is higher than 0.3), irradiated Kapton seems to behave like a heavily doped polymer. The defect centers corresponding to a broad distribution of localized states within the gap consist of single defects, pairs, and small clusters. At this stage, these defects are not necessarily connected into coherent hopping paths. Thus one of the possible conduction mechanisms is just the excitation of the charge carriers occupying the shallowest states in the gap close to the band edge. This hypothesis is consistent with the observed activated behavior $\sigma = \sigma_0 \exp(-\alpha/k_B T)$ with activation energies of a few tenths of eV. It accounts for the conductivities of $10^{-6} \text{ S cm}^{-1}$ or less measured at this stage.

More interesting is the field-dependent dc conductivity which varies like

$$\sigma = \sigma_0 \exp\left(\frac{-\alpha + \beta \sqrt{E}}{k_B T}\right)$$

over a large range of fields E from 100 to 10^6 V cm^{-1} .

In the classical interpretation of the Poole-Frenkel dependence (see for example, the review papers of Hill³¹ and Jonscher and Hill³²), this dependence is due to the lowering of the barrier for escape of the electron by the field. It is important to notice that the \sqrt{E} dependence, in this approach, comes from the Coulombic form of the potential well. Hill shows, for instance, that the lowering produced by the field in a pair of Coulombic wells would lead to a linear E dependence instead of the \sqrt{E} . If we follow closely this interpretation, we should admit that only isolated shallow centers play the major role in the dc conduction in stage II and not the pairs.

Because of the wide applicability of the Poole-Frenkel formula to glassy solids as silicon monoxide SiO_x , boron nitride, amorphous germanium, and even amorphous carbon,³² several authors have tried to extend the applicability of the initial Poole-Frenkel model by exploring less restrictive transport mechanisms than the field-assisted separation of a charge bound in a Coulomb well.

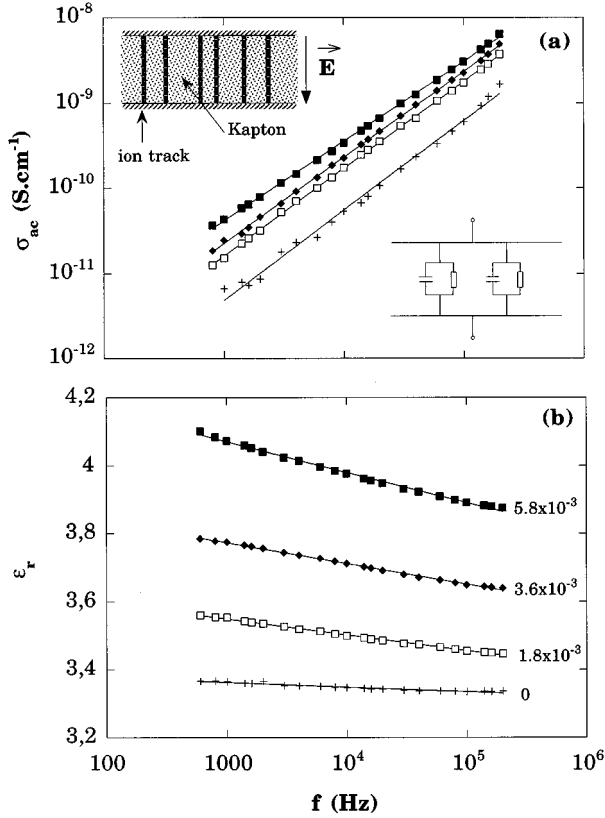


FIG. 5. The increase of the (a) ac conductivity and (b) the dielectric constant (measured under vacuum) in stage I of the transition is well described by a simple effective medium approximation illustrated together with the equivalent circuit in the insets in (a). The irradiation parameters with 60 MeV Cu ions are given in the figure. The ion track is a low-loss inhomogeneous medium with a dielectric constant of around 4. See details in the text.

Their approach, based on Monte Carlo simulations of Miller-Abrahams hopping networks,³³ is more difficult to evaluate in terms of simple physical ideas, and in our case, with our current understanding of the system, the Poole-Frenkel qualitative picture is probably sufficient.

VI. DETAILED DISCUSSION OF THE DIFFERENT STAGES OF THE INSULATOR TO CONDUCTOR TRANSITION

A. Single track stage

This stage corresponds to $\Phi t S_e^2 < 0.003 \text{ Gy}^2 \text{ m}^2$, where the paramagnetic center density is directly proportional to the fluence [Fig. 1(b)]. Here the material exhibits a very anisotropic conductivity due to the existence of individual tracks parallel to each other [upper sketch in Fig. 5(a)]. When measured in the transverse configuration, the dielectric behavior is typical of a simple effective medium symbolized by two parallel RC circuits, the first one corresponding to the ion tracks, the other to the original Kapton matrix [lower sketch in Fig. 5(a)]. Then $\epsilon_{\text{eff}} = (1-P)\epsilon_k + P\epsilon_t$ and $\sigma_{\text{eff}} = (1-P)\sigma_k + P\sigma_t$, where $P = \Phi t \pi R_t^2$ represents the track volume fraction, and (ϵ_k, σ_k) and (ϵ_t, σ_t) are, respectively, the Kapton and the ion track dielectric constants and conductivities. P is calculated using the track radii (R_t)

from Table I. Our results show that the single-ion track is not a conducting wire (even under high electric field) which short-circuits the insulating Kapton matrix. In fact, the track appears as a constant low-loss insulator³⁴ with an effective dielectric constant of around 4, where charges cannot move away, but are very strongly localized. We think that charge localization by spatial disorder arises mainly from the inhomogeneous track morphology. Indeed, neutron and small-angle x-ray scattering data suggest the formation of small particles^{35,36} in such a track.

A single slightly asymmetric inhomogeneous line is observed in X-band and Q-band EPR measurements at RT. A $\Delta H_{\text{p.p.}}$ of 10 G is observed when tracks begin to get in contact [see Fig. 1(b)]. The g factor measured at the crossing of the derivative signal with the base line is about 2.004, rather far from the typical value for π electrons in amorphous carbon.³⁷ Increasing the microwave power level shows that the signal saturates easily in air or inert gas, suggesting a slow spin-lattice relaxation rate T_1 . The study of the saturation curves lead to values of T_1 of the order 10^{-4} s in inert gas and 10^{-3} s in air. We checked that the spin susceptibility versus temperature, obtained by numerical double integration, follows a Curie law up to 500 K. All these ESR results confirm that spins are strongly localized on single sites, pairs, and very small clusters.

B. Onset and growth of the conductivity (stages II and III)

During these two stages, a three-dimensional (3D) random resistor network is progressively built. The building blocks are disordered clusters of π -conjugated bonds, which are created by irradiation inside a single track or in the track overlap regions. In stage II ($0.003 < \Phi t S_e^2 < 0.03$; see Fig. 1), these clusters are too far from each other for a dc hopping path to be established all over the sample. They just act as dopants, and the substrate polymer between the clusters still plays the major role. The frequency dispersion of the dielectric constant and the conductivity reflects that the substrate is inhomogeneous (Fig. 3). In stage III ($0.03 < \Phi t S_e^2 < 0.3$), the hopping network is definitely established and covers the whole sample. It is composed of π -electron-rich clusters where all sites are connected by the high transfer integral t_c (see Sec. V A) and hopping is adiabatic; the clusters are connected to each other by more difficult steps with transfer integrals t_b and nonadiabatic hopping. Then with the reasonable assumptions presented in Sec. V A, it is easy to explain the $\sigma = \sigma_0 \exp[-(T_0/T)^{1/2}]$ dependence for this granular material.¹⁴

The second stage of the transition presents the following characteristics. We checked that transverse and longitudinal conductivities are of the same order of magnitude, which proves the new isotropic character of the material. The dc conductivity is temperature activated [Fig. 2(a)] with an electric field (E) dependence which is Poole-Frenkel like on a very wide range of electric fields [inset of Fig. 2(a)], i.e., $\sigma = \sigma_0 \exp[-(\alpha - \beta E^{1/2})/k_B T]$. The maximum measured activation energy (α) is around 0.3 eV near RT. It is worth noting that electrode effects have been ruled out by varying the size of two samples irradiated to the same fluence and under the same conditions. Such a field dependence is then a real bulk effect, and not an electrode injection Schottky effect. Moreover, Ohmic currents are observed at low dc bias.

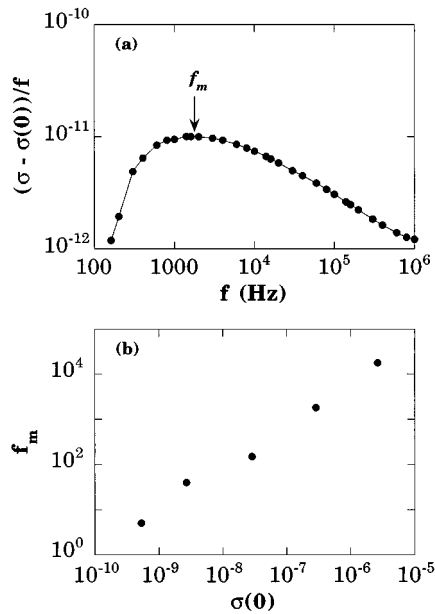


FIG. 6. The presence of a loss peak (a) and the proportionality between the RT loss peak frequency and the RT dc conductivity $\sigma(0)$ suggest that dc and ac conductivities are due to the same mechanisms. These curves have been established from the RT data of σ_{ac} vs frequency, not shown here.

We found that σ_0 is atmosphere dependent. It decreases when dry oxygen or air is allowed in the vacuum chamber. We also observe that water vapor absorption increases the conductivity and the dielectric constant, in contrast with the effects of oxygen. This effect is more pronounced on samples stored in air for a long time.

The experimental β values vary weakly with fluence and atmosphere, but are temperature independent, which is not found in all glassy solids.³⁸ Taking $\epsilon_r \approx 4$ for the dielectric constant, the theoretical Poole-Frenkel $\beta = (e^3 / \pi \epsilon_0 \epsilon_r)^{1/2}$ value should be $0.38 \text{ meV V}^{-1/2} \text{ cm}^{1/2}$. Our values are near $0.25 \text{ meV V}^{-1/2} \text{ cm}^{1/2}$. It is usual to find β values lower than the theoretical ones in amorphous systems.³⁹ We thus believe that in this substage the conductivity is not yet controlled by the growth of clusters, but the damaged polymer behaves as a doped disordered semiconductor, so that the field dependence of the conductivity can be explained by a classical Poole-Frenkel model.

However, in a classical semiconductor, the carrier moves freely in a band and the mobility is quite high so that the ac conductivity is frequency independent (and equal to the dc conductivity). In our case the conductivity increases with frequency [Fig. 3(b)] as in many amorphous semiconductors.³⁴ We found also an increase of the dielectric constant at low frequencies [Fig. 3(a)]. ac conduction in glasses is a long-standing problem, not still completely solved (see, for example, the reviews by Long^{40,41}). An important question is whether or not dc and ac conduction are due to the same mechanism.⁴² When it is the case, a dielectric loss peak should be found and the loss peak frequency f_m should be approximately proportional to the dc conductivity (the so-called Barton-Nakajima-Namikawa relation).⁴² As shown in Figs. 6(a) and 6(b), these two conditions are reasonably met in stage II of the transition.

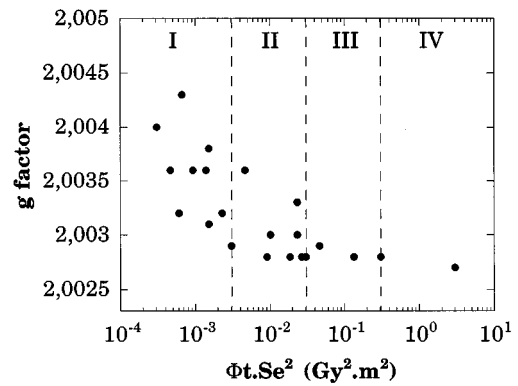


FIG. 7. The g factor is plotted vs the irradiation parameter $\Phi t Se^2$. The decrease towards the π amorphous carbon value (2.0027) illustrates the carbonization process.

Hopping is well known to produce a dispersion in the dielectric response.^{40,41} However, many authors have emphasized that spatial inhomogeneities may give rise to the same behavior in a disordered semiconductor.⁴³⁻⁴⁵ Considering the Poole-Frenkel mechanism which is present in our system in stage II, it is possible here that the dielectric behavior is governed mainly by electrical inhomogeneities, such as potential fluctuations, charged defects, and so on, and not by a microscopic hopping mechanism. The neutral localized states present near the band edges should also affect the ac conduction process by multitrapping effects.⁴⁶ Measurements on a wider frequency range should be performed to clarify this point.

When $\Phi t Se^2 < 0.03$ (stage III), RT conductivity increases gradually with the damage. The temperature dependence is of the type $\sigma = \sigma_0 \exp[-(T_0/T)^{1/2}]$, over many orders of magnitude [Fig. 2(b)]. This behavior is typical in granular disordered solids, which arises from Coulomb interactions (via the charging energy).³⁰ The carriers are self-trapped on disordered structures rich in π bonding. The high electronic-transfer integrals which link the carbon atoms of the grains ensure a fast adiabatic hopping within the grain while inter-grain hopping is nonadiabatic. We found that T_0 decreases with fluence, but increases when oxygen comes into contact with the porous solid. T_0 values as high as $1.4 \times 10^5 \text{ K}$ have been measured for air-exposed samples.

Following the ESR data, all along stages II and III, we start from a nearly Lorentzian homogeneously narrowed line. A decrease of the g value from 2.004 in stage I to 2.0028 is also observed (Fig. 7). The inhomogeneous character of the line completely disappears with increasing fluence, and the line shape becomes more and more Lorentzian. This behavior is observed even at helium temperature, where dc hopping conduction is frozen out. Therefore, we suggest that exchange interactions should be responsible for such narrowing at low temperature.^{47,19} The temperature dependence of the spin susceptibility still exhibits a Curie-like behavior up to 500 K (there is no evidence of any Pauli-like contribution here). These results demonstrate that ESR is the best method to follow the growth of the conducting clusters in irradiated polymers. The narrowing of the line and the decrease of the g value are obviously due to the presence of more and more conjugated bonds along the spin paths.

When air is allowed in the quartz tube, the number of spins is reduced by at least a factor of 3 and $\Delta H_{p.p.}$ increases from 1 G to a value between 2 and 6 G: the lower the paramagnetic center density, the larger the $\Delta H_{p.p.}$ in air. This effect is partially reversible. The double-cavity technique permits an accurate verification that no g -value shift appears when air or oxygen is admitted. The spin-lattice relaxation time increases in air or pure oxygen. In fact, we observed that the lower the spin density and sample dc conductivity, the higher the spin-lattice relaxation time.¹⁹ Theoretical descriptions of linewidth narrowing and spin-lattice relaxation induced by spin-spin interactions and hopping motion have been treated separately by several authors.^{48,49} Our opinion is that critical 3D paths must exist for the spin diffusion in the interacting spin system, in the same way as for charge conduction. Spin and charge diffusion are both determined by random walks on a random network. If critical bonds are suppressed in the paths, this would affect the entire system, because distributions are more important than averages in random solids.

C. Comparison of the transport properties in stages II and III to those of granular metal films

It is striking to realize that both regimes observed during the growth of the conductivity in irradiated Kapton have been also found in granular metals.⁵⁰ In his famous review on granular metal films produced by coevaporation of metals and oxides, Abeles mentioned that measurements on discontinuous films by Neugebauer and Webb⁵¹ indicate both an activated temperature dependence of the conductivity and a Poole-Frenkel field dependence. The values of the conductivities and of the parameters of the models are the same orders of magnitude as in the first part of stage II here.

The famous $\exp[-(T_0/T)^{1/2}]$ that we found (as did many other authors) in the second part of stage II is also typical of the continuous granular films of Abeles (and co-workers). One may wonder if phonon-assisted tunneling between the metal clusters could explain the dependences in both regimes.

Like Abeles, we believe that it is not the case. In discontinuous films like in the first part of our stage II, the clusters are so disconnected from each other that they play essentially no role. What we observed is a substrate conductivity typical of a disordered polymer in which the creation of the charge carrier from a dopant center is the difficult step and the granularity plays a negligible role. On the contrary, in continuous percolated films like in the second part of our stage II, phonon-assisted tunneling between the "metallic" clusters plays the main role.

D. Adiabatic conduction stage

At high fluence ($\Phi tSe^2 > 0.3$), σ_{dc} approaches 100 S cm^{-1} and becomes weakly temperature dependent. The unpaired electron density D_v starts decreasing with irradiation. The g value is still near 2.0027, but $\Delta H_{p.p.}$ increases drastically both with the damage and the temperature (Fig. 8). Moreover, the line wings are broader than those of a Lorentzian line (inset in Fig. 8). Oxygen-free samples must be chosen for these experiments, since a broadening of the line and a decrease in paramagnetic center density are still observed in

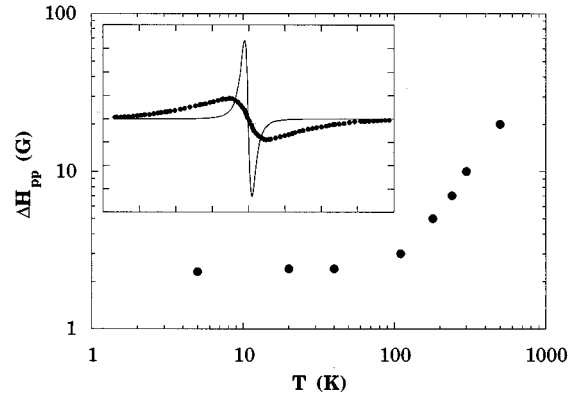


FIG. 8. Temperature dependence of $\Delta H_{p.p.}$ in stage-IV material. The increase of $\Delta H_{p.p.}$ vs temperature (T) for the dotted line is linked to the conductivity increase as in metals. The inset shows the experimental line shape (solid circles) compared to the solid Lorentzian line with a $\Delta H_{p.p.}$ of 4 G. The broad wings are expected to be due to a distribution of relaxation times.

air-exposed samples. For samples stored in air during several days, the ESR signal becomes hardly detectable. However, oxygen diffusion is slow compared to the previous stage and enhanced by heating above RT, which confirms that a structural densification took place, with a decrease of the porosity.

An interesting comparison can be made with pyrolyzed Kapton, in which most of these features are also present at pyrolysis temperatures situated between 900 and 2000 °C and for a sufficient treatment time.^{2,52-54} The maximum conductivity is around 100 S cm^{-1} . A further increase can be obtained only above 2000 °C when graphitization sets in. A dramatic drop of the paramagnetic center density is also observed above 600 °C. Moreover, a Pauli-like component appears in the magnetic susceptibility of these pyrolyzed samples together with the Curie term.

It is tempting, in pyrolyzed as well as strongly irradiated samples, to attribute these features to a significant concentration of metallic graphitic grains created during the local rearrangement of the carbonaceous disordered material. However, this interpretation is not applicable to the results on highly irradiated Kapton presented here. A true polycrystalline graphite should give rise to a motionally narrowed isotropic line ($\Delta H_{p.p.} \leq 4 \text{ G}$) at high temperature, and the susceptibility should increase very slightly.⁵⁵ For sample 3 in Fig. 4, the presence of a 4-G Lorentzian line corresponding to 10% graphite could be resolved (solid line in the inset of Fig. 8). Moreover, the susceptibility follows a Curie law between 4 and 200 K, and increases strongly when $T > 200 \text{ K}$.

We note that the spin susceptibility measurements reported in Fig. 4 have been performed on well-outgassed samples in sealed tubes under He atmosphere. The ESR behavior is found to be perfectly reversible between 300 and 500 K, which eliminates the possibility that the high-temperature increase could be due to oxygen desorption.

Indeed, conducting electrons are still localized in the entire homogeneously disordered samples. But the large number of π -conjugated bonds ensures the existence everywhere of transfer integrals of the order of 2–3 eV, much larger than the typical phonon energies for hopping. Although order is not sufficient to ensure coherent conduction like in a metal,

TABLE II. Main characteristics of the insulator-conductor transition in poly(imide) Kapton-H as a function of the irradiation parameter $\Phi t S e^2$. dc conductivity (σ_{dc}), with temperature (T) dependence. ESR behavior, with peak-to-peak line width ($\Delta H_{p.p.}$), g value, and temperature dependence of the susceptibility [$\chi(T)$] (see text for symbols).

	σ_{dc}	$\sigma_{dc}(T)$	$\Delta H_{p.p.}$ (G) at RT	g	$\chi(T)$	Mechanical properties	Color
Stage I ($\Phi t S e^2 \leq 0.003$)	≈ 0	≈ 0	≈ 8	2.004	Curie	still plastic	brown
Stage II ($0.003 \leq \Phi t S e^2 \leq 0.03$)	Power law vs irradiation parameter $\propto (\Phi t S e^2)^{12}$ + Poole-Frenkel field dependence $\propto \exp(\beta \sqrt{E}/k_B T)$	Activated $\exp(-\alpha/k_B T)$	decreases towards 1 G	decrease	Curie	loss of plasticity but still not brittle	black, mat
Stage III ($0.03 \leq \Phi t S e^2 \leq 0.3$)	saturation sets in (decrease of the exponent in the power law)	$\exp[-(T_0/T)^{1/2}]$ T_0 decreases with irradiation	1	2.0028	Curie	brittle (volume contraction)	black, metallic lustre
Stage IV ($0.3 \leq \Phi t S e^2$)	saturation $\approx 100 \text{ S cm}^{-1}$	decrease only at low T	increases up to 10 G and more	2.0027	Curie+triplet	brittle	black, metallic lustre

the transfer integrals are large enough to guarantee an efficient adiabatic hopping of a large number of carriers to pervade in the sample.^{26,27} Here electron transport just follows the transport of vibrational energy. Carriers act as slaves of phonons, thus leading, at high temperature, to a rather temperature-independent conductivity.^{56,57} We are not surprised that such a regime also leads to an ESR linewidth that increases with temperature just like in a metal. This has been already explained in disordered semiconductors by Movaghar, Schweitzer, and Overhof.⁴⁹

The disordered metal hypothesis has been invoked by Venkatesan *et al.* to explain the high Hall carrier density and the small thermopower of irradiated amorphous carbon and polymers.⁵⁸ Their (TEM) transmission electron microscopy observations show that a kind of graphitic ordering with very short correlation length is created. Earlier on, Mrozovsky noticed that strong deviations appear in the ESR and electronic properties of graphite when the crystallite size becomes nanometric.⁵⁹ Regarding the structural information, we found no evidence of graphitic TEM diffraction patterns appearing for the highly irradiated samples.⁶⁰

Following Emin and Bussac^{61,62} we suggest that structural defects and distortion of the C-C covalent bonds in graphitic-like amorphous carbon can induce polaronic collapse of the carrier wave functions. If the on-site Coulomb repulsion U is not too high (as is the case in conducting polymers, i.e., about 1 eV), then spinless bipolarons could form and thus the increase of the susceptibility at high temperature could arise from excited triplet states of bipolarons. Samples 2 and 3 of Fig. 4 have been fitted with the sum of Curie (polarons) and excited triplet (bipolarons) components with a reasonable exchange energy $J = 1000 \text{ K}$:

$$\chi = \frac{N_p \mu_b^2}{k_B T} + \frac{N_b \mu_b^2}{k_B T} \frac{4}{3 + \exp(2|J|/k_B T)}$$

N_p and N_b are, respectively, the polaronic and bipolaronic carrier density. The least-squares fit gives $N_b/N_p \approx 70$ for sample 3 and $N_b/N_p \approx 9$ for sample 2: i.e., N_b/N_p increases with the irradiation parameter ($\Phi t S e^2$). We found also $N_b + N_p \approx 10^{21} \text{ cm}^{-3}$, which fixes a lower limit for the total

carrier density. In fact, N_b is expected to be higher because bipolarons with higher exchange energies ($J > 1000 \text{ K}$) should also be present. A more realistic fit should take into account a distribution of J values.

A similar situation is encountered in disordered conducting polymers when the dopant concentration increases.^{14,63-65} The equilibrium between polarons and bipolarons arises from fluctuations in the local carrier density. It is worth noting that a spin-dependent low-temperature conductivity is found in both systems by magnetoresistance measurements.^{14,66}

In this disordered polaron-bipolaron glass picture, despite the high conductivity, the ESR line is inhomogeneous with large wings (see inset in Fig. 8), which arise from a wide distribution of spin-lattice relaxation times. In a real metal, fast diffusion should give a pure homogeneous Lorentzian line.

The different characteristics of the four stages are summarized in Table II, showing the major relevant parameters of the insulator-conductor transition.

VII. CONCLUSIONS

The conducting properties of heavy-ion irradiated poly(imide) Kapton-H are determined by the formation of a disordered granular carbonaceous structure. The latter process takes place along four stages.

At low fluence, in stage I, the damage is localized in the individual ion tracks. A high-density energy threshold for damage of 14 eV nm^{-3} is found and explains the poor efficiency of electron beams. No significant dc conduction is found during this single-track stage; i.e., the track is not a conducting wire. The ESR line is observed to be partly inhomogeneous, with slow spin-lattice relaxation and spin diffusion rates.

With increasing fluence, in stages II and III, a 3D π -cluster structure is formed when tracks get in contact. At the beginning, in stage II, the clusters are too far away and they just act as dopants for the damaged polymeric matrix. The conduction process is Poole-Frenkel like. In stage III, transfer integrals between clusters are weak, and dc conduc-

tion takes place by nonadiabatic hopping between nearest-neighbor charged and neutral clusters. Molecular oxygen can be used as a probe for spin and charge dynamics, which are found to be strongly correlated. Both spin diffusion and dc conductivity appear simultaneously along critical paths in the random 3D cluster network.

At higher fluence, in stage IV, true percolation between large π clusters takes place, and the low-temperature narrowing of the ESR line by small exchange interactions is replaced by a temperature-dependent adiabatic hopping-induced broadening. The dc conductivity saturates at high temperatures near 100 S cm^{-1} , but slightly decreases at low temperature.

The disordered adiabatic carbonaceous regions created by irradiation are rich in graphitic sp^2 bonding and should have a high finite density of states near the Fermi level. Following Emin and Bussac,^{61,62} we suggest that the structural disorder can induce polaron and bipolaron formation in these covalent materials with short-range electron-lattice interactions by a feedback effect. The disorder energy needed to form polarons is much reduced compared to the Anderson criterion

of localization. This suggests that no quasifree carrier can exist in these disordered "graphitic" structures. Instead, a polaron-bipolaron glass is created. Thus, in many aspects, irradiated Kapton is an intermediate system between conducting polymers and disordered graphite.

This qualitative model reconciles many observations by different groups and constitutes an alternative explanation of the insulator-conductor transition in irradiated or pyrolyzed organic solids, where a significant microscopic structural disorder precludes the presence of a true graphitic ordered phase.

ACKNOWLEDGMENTS

We are indebted to S. Esnouf, F. Beuneu, and P. Vajda (Ecole Polytechnique, France) for low-temperature ESR and conductivity measurements and also for many stimulating discussions. We would like to thank also O. Chauvet (EPFL, Switzerland) for Q -band measurements and helpful discussions. L. Forro and D. Romero (EPFL, Switzerland) are also acknowledged for a reading of the manuscript.

*Present address: Ecole Polytechnique Fédérale de Lausanne (IGA/DP), CH-1015 Lausanne, Switzerland.

¹E. Fitzer, K. Mueller, and W. Schaeffer, in *Chemistry and Physics of Carbon*, edited by P. L. Walker, Jr. and P. A. Thrower (Dekker, New York, 1971), Vol. 7, p. 237.

²S. D. Bruck, *Polymer* **6**, 319 (1965).

³S. R. Forrest, M. L. Kaplan, P. H. Schmidt, W. L. Feldmann, and E. Yanowski, *Appl. Phys. Lett.* **41**, 90 (1982).

⁴T. Venkatesan, L. Calcagno, B. S. Elman, and G. Foti, in *Ion Beam Modification of Insulators*, edited by P. Mazzoldi and G. W. Arnolds (Elsevier, Amsterdam, 1987), p. 301.

⁵H. B. Brom, Y. Tomkiewicz, A. Aviram, A. Broers, and B. Sunners, *Solid State Commun.* **35**, 135 (1980).

⁶A. J. Heeger, S. Kivelson, J. R. Schrieffer, and W.-P. Su, *Rev. Mod. Phys.* **60**, 781 (1988).

⁷D. Baeriswyl, D. K. Campbell, and S. Mazumdar, in *Physics of Conducting Polymers*, edited by H. Kiess (Springer-Verlag, Berlin, 1992), p. 7.

⁸B. Wasserman, G. Braunstein, M. S. Dresselhaus, and G. E. Wnek, in *Ion Implantation and Ion Beam Processing of Materials*, edited by G. K. Hubler, O. W. Holland, C. R. Clayton, and C. W. White, MRS Symposium Proceedings No. 27 (North-Holland, New York, 1984), p. 413.

⁹M. L. Kaplan, S. R. Forrest, P. H. Schmidt, and T. Venkatesan, *J. Appl. Phys.* **55**, 732 (1984).

¹⁰D. Emin, *Phys. Rev. Lett.* **32**, 303 (1974).

¹¹L. S. Singer, *Proceedings of the Fifth Carbon Conference* (Pergamon, New York, 1962), p. 37.

¹²M. Nechtschein and F. Genoud, *Solid State Commun.* **91**, 471 (1994).

¹³S. Fujimori, K. Hoshimono, and S. Fujita, *Solid State Commun.* **89**, 437 (1994).

¹⁴L. Zuppiroli, M. N. Bussac, S. Paschen, O. Chauvet, and L. Forro, *Phys. Rev. B* **50**, 5196 (1994).

¹⁵T. Hioki, S. Noda, M. Sogiura, M. Kakeno, K. Yamada, and J. Kawamoto, *Appl. Phys. Lett.* **43**, 30 (1983).

¹⁶S. Noda and T. Hioki, *Carbon* **22**, 359 (1984).

¹⁷J.-M. Constantini, J. L. Flament, V. Mori, L. Sinopoli, J. Trochon,

J. L. Uzureau, L. Zuppiroli, L. Forro, J. Ardonneau, and D. Lesueur, *Radiat. Eff. Defects Solids* **115**, 83 (1990).

¹⁸J.-P. Salvetat, A. Berthault, F. Brisard, J. M. Costantini, and J. Davenas, *Radiat. Eff. Defects Solids* **136**, 267 (1995).

¹⁹J.-P. Salvetat, J.-M. Costantini, and F. Brisard, *Nucl. Instrum. Methods B* **116**, 284 (1996).

²⁰J. P. Biersack and L. G. Haggmark, *Nucl. Instrum. Methods* **174**, 257 (1980).

²¹B. Wassermann, *Phys. Rev. B* **34**, 1926 (1986).

²²J. Frenkel, *Phys. Rev.* **54**, 657 (1938).

²³J. L. Hartke, *J. Appl. Phys.* **39**, 4871 (1968).

²⁴N. F. Mott, *J. Non-Cryst. Solids* **1**, 1 (1968).

²⁵A. L. Efros and B. I. Shklovskii, *J. Phys. C* **8**, L49 (1975).

²⁶T. Holstein, *Ann. Phys. (N.Y.)* **8**, 325 (1959).

²⁷D. Emin, *Phys. Rev. B* **43**, 11 720 (1991); **46**, 9419 (1992); **48**, 13 691 (1993).

²⁸A. Miller and E. Abrahams, *Phys. Rev.* **120**, 745 (1960).

²⁹V. Ambegaokar, B. I. Halperin, and J. S. Langer, *Phys. Rev. B* **4**, 2612 (1971).

³⁰Ping Sheng, B. Abeles, and Y. Arie, *Phys. Rev. Lett.* **31**, 44 (1973).

³¹R. M. Hill, *Philos. Mag.* **23**, 59 (1971).

³²A. K. Jonscher and R. M. Hill, in *Physics of Thin Films*, edited by G. Hass, M. H. Francombe, and R. W. Hoffman (Academic, New York, 1975), p. 169.

³³M. Abkowitz, H. Bassler, and M. Stolka, *Philos. Mag. B* **63**, 201 (1991).

³⁴A. K. Jonscher, in *Physics of Thin Films* (Academic, New York, 1980), Vol. 11, p. 205.

³⁵D. Fink, K. Ibel, P. Goppelt, J. P. Biersack, L. Wang, and M. Behar, *Nucl. Instrum. Methods B* **46**, 342 (1990).

³⁶O. Yu. Posudievsky, *Radiat. Eff. Defects Solids* **137**, 119 (1995).

³⁷R. J. Gambino and J. A. Thompson, *Solid State Commun.* **34**, 15 (1980).

³⁸M. Abkowitz, M. J. Rice, and M. Stolka, *Philos. Mag. B* **61**, 25 (1990).

³⁹A. K. Jonscher, *J. Phys. C* **4**, 1331 (1971).

⁴⁰A. R. Long, *Adv. Phys.* **31**, 553 (1982).

- ⁴¹A. R. Long, in *Hopping Transport in Solids*, edited by M. Pollak and B. Shklovskii (Elsevier, New York, 1991), p. 207.
- ⁴²J. C. Dyre, *J. Non-Cryst. Solids* **135**, 219 (1991).
- ⁴³R. Stumpe, *Phys. Status Solidi A* **88**, 315 (1985).
- ⁴⁴A. R. Long, *Philos. Mag. B* **59**, 377 (1989).
- ⁴⁵J. C. Dyre, *Phys. Rev. B* **48**, 12 511 (1993).
- ⁴⁶J. Noolandi, *Phys. Rev. B* **16**, 4474 (1977).
- ⁴⁷P. W. Anderson and P. R. Weiss, *Rev. Mod. Phys.* **25**, 269 (1953).
- ⁴⁸P. W. Anderson, *J. Phys. Soc. Jpn.* **9**, 316 (1954).
- ⁴⁹B. Movaghar, L. Schweitzer, and H. Overhof, *Philos. Mag. B* **37**, 683 (1978).
- ⁵⁰B. Abeles, *Advances in Materials and Device Research*, Applied Solid State Science (Academic, New York, 1976), p. 53.
- ⁵¹C. A. Neugebauer and M. B. Webb, *J. Appl. Phys.* **33**, 74 (1962).
- ⁵²O. Chauvet, L. Zuppiroli, and I. Safi (unpublished).
- ⁵³C. Z. Hu, K. L. DeVries, and J. D. Andrade, *Polymer* **28**, 663 (1987).
- ⁵⁴M. Inagaki, S. Harada, T. Sato, T. Nakajima, Y. Horino, and K. Morita, *Carbon* **27**, 253 (1989).
- ⁵⁵G. Wagoner, *Phys. Rev.* **118**, 647 (1960).
- ⁵⁶F. Rullier-Albenque, L. Zuppiroli, and F. Weiss, *J. Phys. (Paris)* **45**, 1689 (1984).
- ⁵⁷D. Belitz and W. Schirmacher, *J. Phys. C* **16**, 913 (1983).
- ⁵⁸T. Venkatesan, R. C. Dynes, B. Wilkens, A. E. White, J. M. Gibson, and R. Hamm, *Nucl. Instrum. Methods B* **1**, 599 (1984).
- ⁵⁹S. Mrozovsky, in *Proceedings of the Fifth Carbon Conference* (Pergamon, New York, 1962), p. 79.
- ⁶⁰M. Caput and J.-P. Salvétat (unpublished).
- ⁶¹D. Emin and M.-N. Bussac, *Phys. Rev. B* **49**, 14 290 (1994).
- ⁶²M.-N. Bussac, G. Mamalis, and P. Mora, *Phys. Rev. Lett.* **75**, 292 (1995).
- ⁶³M. N. Bussac and L. Zuppiroli, *Phys. Rev. B* **47**, 5493 (1993).
- ⁶⁴O. Chauvet, S. Pachen, M. N. Bussac, and L. Zuppiroli, *Europhys. Lett.* **26**, 619 (1994).
- ⁶⁵P. K. Kahol, W. R. Spencer, N. J. Pinto, and B. J. McCormick, *Phys. Rev. B* **50**, 18 647 (1994).
- ⁶⁶A. N. Aleshin and A. V. Suvorov, *Philos. Mag. B* **65**, 783 (1992).